



Physical properties of biomass-derived novel natural deep eutectic solvents based on choline chloride and (*R*)-3-hydroxyacids

Lyall Archer^a, Barbara Jachimska^b, Marcel Krzan^b, Maciej Szaleniec^b, Edyta Hebda^c, Paulina Radzik^c, Krzysztof Pielichowski^c, Maciej Guzik^{b,*}

^a Department of Chemical & Process Engineering, University of Strathclyde, 75 Montrose Street, Glasgow G1 1XJ, United Kingdom

^b Jerzy Haber Institute of Catalysis and Surface Chemistry Polish Academy of Sciences, Niezapominajek 8, 30-239 Krakow, Poland

^c Department of Chemistry and Technology of Polymers, Cracow University of Technology, ul. Warszawska 24, 31-155 Krakow, Poland

ARTICLE INFO

Article history:

Received 19 February 2020

Received in revised form 17 June 2020

Accepted 24 June 2020

Available online 2 July 2020

Keywords:

Natural deep eutectic solvents

(*R*)-3-hydroxyacids

Polyhydroxyalkanoate

Choline chloride

Viscosity

Density

ABSTRACT

We report the synthesis and physicochemical characterization of a series of Natural Deep Eutectic Solvents (NADESs), a subclass of ionic liquids that have demonstrated their potential as green solvents for widespread commercial application, including bio-safe chemical engineering technologies. The novel NADESs comprise of hydrogen bond donating (HBD) (*R*)-3-hydroxyalkanoic acids (R3HAs), biodegradable monomers of renewable polymer polyhydroxyalkanoate (PHA), and an appropriate conjugate hydrogen bond acceptor (HBA) species; namely choline chloride (ChCl). We combined theoretical and experimental methods to characterize a series of NADESs with increasing content of R3HAs. Gas-phase theoretical modelling provided insight on potential hydrogen bond interactions between the components of the novel NADES and facilitated interpretation of their IR and ¹H NMR spectra. The experiments revealed that the viscosity of R3HA:ChCl NADESs increased with decreasing temperature and increasing fraction of ChCl. The viscosity-temperature dependence was best described by a polynomial relationship; the Vogel-Tamman-Fulcher (VTF) model was also used but did not represent the empirical data, suggesting R3HA:ChCl NADES's viscosity-temperature behaviour is of non-Arrhenius type. Similarly, density was shown to increase with decreasing temperature and increasing ChCl fraction. In contrast to viscosity, the bonding ratio change was found to have little effect on density at a fixed temperature, other than the proportional increase associated with a higher fraction of the denser component. Solubility and wettability investigations concluded that R3HA:ChCl NADESs are compatible with mildly polar and hydrophobic solvents and as a result have a polarity index in the range 0–4.1.

© 2020 Elsevier B.V. All rights reserved.

1. Introduction

Over the recent years, significant amounts of work have been dedicated to the development of environmentally friendly solvents. One example of a family of these new species is Natural Deep Eutectic Solvents (NADES), which are both biodegradable and non-cytotoxic [1]. NADES are two or three-component mixtures of hydrogen bond acceptors and hydrogen-bond donors, derived from primary metabolites (e.g. organic fatty acids, amines, amino acids, sugars or phenolic compounds). These green solvents are gaining more and more attention in the scientific community and industry. Various areas of their application are proposed. For example, they have found the right place in biorefining processes as solvents for selective extraction of biomass components or its initial pretreatment [2–5]. NADES are also proposed to serve as suitable media in catalysis [6], biocatalysis [7–9] and polymer chemistry [10].

Considering sustainable development principles, the NADES components should be obtained from bio-based and renewable resources. Choline chloride and biomass-derived fatty acids appear to be the ideal candidates; their mixtures have been shown to form NADES [11–13], however, with some limitations. When one considers the generation of NADES with choline chloride and aliphatic fatty acids of medium chain length carbon backbone, it may be impossible to achieve a liquid phase up to 373 K. Nevertheless, liquefaction may occur when more hydrogen bond interactions are facilitated between NADES components [14]. For this purpose, hydroxylated fatty acids may serve as HBD, thus offering generation of systems with desired properties.

In our work we have focused on the development of a series of NADES that take into consideration all of the above. In order to obtain hydroxylated fatty acids, we have utilised bacterially derived polymers – polyhydroxyalkanoates (PHAs), which in nature are polyesters of (*R*)-3-hydroxylated fatty acids [15]. Bacteria can synthesise these polymers from virtually any carbon source producing a range of PHAs with various structures [16]. For example, *Pseudomonas* spp. accumulate medium chain length PHAs from biomass-derived carbon sources like

* Corresponding author.
E-mail address: ncguzik@cyfronet.pl (M. Guzik).

sugars, vegetable oils, glycerol or long-chain length fatty acids [17]. When grown on these substrates, they produce PHAs polymers that contain a mixture of (*R*)-3-hydroxylated fatty acids ranging from 6 to 14 carbon atoms in their chains [18,19]. Here we have used such a mixture that originated from PHA polymer of *Pseudomonas putida* CA-3 cells grown on rapeseed oil-derived fatty acids to prepare NADES with choline chloride in different ratios of HBD to HBA. We have then analysed these mixtures in order to understand the influence of each component on their physiochemical characteristics. Firstly, we present theoretical studies of possible HBA and HBD interactions basing on gas-phase theoretical modelling. Further, a detailed investigation is presented on temperature dependence on the viscosity and density of the new NADES. Finally, we provide results of a solubility screening of NADES in common solvents.

2. Experimental

2.1. Materials

Polyhydroxyalkanoate (PHA) was produced with *Pseudomonas putida* CA-3 strain with fatty acids derived from rapeseed oil hydrolysis as the sole energy and carbon source; extracted with ethyl acetate and characterised as in our previous manuscript [20]. The polymer was degraded to its monomeric units via an acidic methanolysis, followed by saponification with LiOH [21] to yield free hydroxylated fatty acids (HAs) – a mixture of (*R*)-3-hydroxyhexanoic, (*R*)-3-hydroxyoctanoic, (*R*)-3-hydroxydecanoic, (*R*)-3-hydroxydodecanoic, (*R*)-3-hydroxydodecenoic and (*R*)-3-hydroxytetradecanoic acids in the molar ratio of 4.0 to 33.7 to 31.8 to 5.0 to 6.4 to 19.1, respectively. Choline chloride ([Ch]Cl) was purchased from Merck, Poland and was of synthesis grade, similar to all other chemicals used in this study. The molecular weight of 190.42 g/mol was calculated based on R3HAs distribution in the synthesized polymer. It was used for calculating the amounts of hydrogen bond donor (HBD) to hydrogen bond acceptor (HBA). Deep Eutectic Solvents (DESs) were constructed by mixing donor to the acceptor in molar ratios of 1:1, 1.5:1, 2:1, 2.5:1 or 3:1, heated to 333 K in order to speed up the solubilisation. Preparation of 1:1 and 1.5:1 R3HAs to choline chloride DESs required ~3 h of mixing and heating at 333 K, whereas the other DESs liquefied relatively quickly at the same conditions (~30 min). The mixtures were stored at room temperature for further experiments.

2.2. Theoretical calculations and model assumptions

The geometries of choline chloride and (*R*)-3-hydroxyhexanoic 1:1, 2:1, 3:1 and 4:1 complexes, as well as DES substrates (i.e. choline chloride, isolated (*R*)-3-hydroxyhexanoic acid and its dimer), were modelled in the gas-phase using Gaussian 16.E.01. The different starting geometries were optimized within density functional theory according to the two-stage protocol. At the first stage the geometries were optimized using spin restricted B3LYP [22] and 6-31g+(2d,2p) contracted Gaussian basis set [23]. The resulting geometries were re-optimized using B3LYP and 6-311++g(2d,2p) basis set with D3 empirical dispersion correction [24]. The thermochemical corrections were obtained from vibrational calculations performed on the B3LYP-D3/6-311++g(2d,2p) level of theory without scaling factor. The ΔG values of complex formation were calculated as a difference between G of complex and G_s of component substrates. The obtained binding Gibbs free energies were corrected for the base superposition errors (BSSE). The identification of H-bond was based on geometry analysis as well as on detection of the redshift of the O—H stretching modes obtained from vibration calculations. The IR frequencies were corrected by a scaling factor of 0.967, according to the Computational Chemistry Comparison and Benchmark DataBase of NIST Standard Reference Database (ver. 20, August 2019). The NMR spectra were calculated using the Gauge-Independent Atomic Orbital (GIAO) method [25] and the obtained

results were referred to TMS shift (31.8821 ppm) calculated at B3LYP/6-311+G(2d,p) level of theory.

2.3. Nuclear magnetic resonance (^1H NMR)

^1H NMR spectra were obtained in CDCl_3 with tetramethylsilane as the internal standard using a 300 Hz spectrometer (Bruker BioSpin GmbH). Number of scans: 56; pulse width: 14.5 s; acquisition time: 3.5 s.

2.4. Attenuated total reflection Fourier transform infrared (ATR-FTIR)

ATR-FTIR analyses were performed using a Nicolet iS5 spectrometer equipped with a diamond crystal attenuated total reflectance unit from Thermo Electron Corporation. Spectra were recorded with a resolution of 4 cm^{-1} from 4000 to 400 cm^{-1} as an average of 16 scans.

2.5. Thermogravimetric analysis (TGA)

Thermogravimetric analyses were carried out using a STA 449 F3 Jupiter analyzer (Netzsch, Selb, Germany). Samples of about 5.5 mg were placed in open Al_2O_3 crucibles and heated in the dynamic mode at a heating rate of 10 K/min, in the temperature range of 303–413 K in argon atmosphere.

2.6. Differential scanning calorimetry (DSC)

DSC was performed using Mettler-Toledo DSC 822 analyzer. Each sample of around 5.5 mg was weighed in the aluminum pan and tightly sealed. Analyses were carried out in an argon atmosphere. Samples were cooled down to 233 K, kept isothermally for 15 min and then heated to 293 K at a heating rate of 10 K/min.

2.7. Density and viscosity measurements

The densities of solutions were measured using the DMA 5000 M densitometer (Anton Paar), which is based on the oscillating U-tube method with a measurement accuracy of $5 \times 10^{-6}\text{ g/cm}^3$. All measurements were conducted in a temperature range of 298–333 K. The temperature was controlled to $\pm 0.005\text{ K}$. Dynamic and kinematic viscosities were measured using a Lovis 2000 M/ME rolling ball microviscometer (Anton Paar). Dynamic viscosity of the sample (η) is calculated using the mean rolling time (tr), the density of the sample and the ball (ρ_s and ρ_b) and a proportionality constant (K) according to equation $\eta = K(\rho_b - \rho_s)tr$. The value of K results from adjustment of the equipment to a reference viscosity standard. The diameter of the glass capillary was 2.5 mm. The apparatus was calibrated before measurements using N100 oil as a viscosity standard. The apparatus measured viscosity in the range from 0.3 to 10,000 mPa·s with an accuracy of 0.05%. All measurements were conducted in the temperature range of 303–333 K.

2.8. Dynamic contact angle measurements

The dynamic contact angles between studied DESs and flat surfaces of different polarity (Teflon, glassy carbon and mica) were measured using a Drop Shape Analyzer KRÜSS DSA100M instrument (Hamburg, Germany, GmbH). Sterile syringe needles (stainless steel, NE 44, KRÜSS, GmbH) were used for each new measurement in manual mode. The instrument recorded images with a digital camera (200 fps), which were further processed using a digital image processing algorithm to calculate the droplet's contact angle by tangents approximations. Measurements were conducted under constant temperature ($295.15 \pm 0.6\text{ K}$) and humidity. For each sample, at least five successive measurements were conducted. In the case of mica, we used fresh surfaces, produced immediately after separation of the mineral layers.

Teflon and glassy carbon surfaces were cleaned with isopropanol and pure water (Merck Millipore Simplicity ultrapure water, resistivity 18.2 M Ω cm, surface tension 72.8 mN/m at 293.15 K) immediately before the experiment. The surfaces of these materials were dried in the flow of pure argon (99.999%).

2.9. Solubility of DESs

To measure the solubility of a DES in a solvent (water, *n*-hexane, chloroform or methanol), one part of DES was mixed with either 3, 4 or 5 parts of a solvent in a 1.5 ml capsule by vigorous mixing for 60s in a laboratory vortex (IKA, Poland). Next, the capsule was centrifuged in microcentrifuge (MPW, Poland) at 14500 RPM for 10 min. Aliquots of the sample's solvent layer (1 ml) was pipetted into a fresh, pre-weighed capsule and incubated in a Thermo-Shaker TS-100C (Biosan, Latvia) at 1000 RPM, 333 K for 24 h, allowing the solvent to slowly evaporate. The capsule was removed from the incubator and weighed to determine the mass of residual DES.

3. Results and discussion

3.1. Deep eutectic solvents synthesis

PHA polymer from bacterial fermentation of rapeseed oil free fatty acids was converted to free hydroxylated fatty acids (R3HAs), which served as hydrogen bond donors (HBD) for preparation of DES with choline chloride. All of the prepared DESs were slightly yellow in colour. Results obtained from TG analyses showed there was no significant mass loss at around 373 K, which could have been associated with water evaporation. However, percentage weight loss in the temperature range of 303–393 K for 3:1, 2.5:1, 2:1, 1.5:1 and 1:1 samples were 2.9, 1.4, 3.0, 2.3 and 1.5%, respectively (Fig. S1). It could have been associated with the presence of volatile compounds in the samples. Further, DSC analyses revealed that there were no endothermic peaks at around 273 K which could have been associated with the melting of the free water crystals if present in the samples (Fig. S2). Moreover, the obtained scans were almost flat in the investigated ranges (243–293 K) without any thermal events. At temperatures below the water freezing point, DSC curves did not show any peaks, evidencing the absence of freezable bound water [26].

3.2. Theoretical modelling of DESs

The quantum mechanical modelling provided insight into possible molecular interactions between NADES components and the basis for an interpretation of the experimental NMR and IR spectra. In this modelling study we considered 1:1, 2:1, 3:1 and 4:1 (*R*)-3-hydroxyhexanoic acid:choline complexes. Two basic geometries of the 1:1 complexes were observed: i) with the carboxyl group of the fatty acid pointing toward Cl⁻ ion and OH group of the choline (Fig. 1A – **complex 1:1a**) and ii) with carboxyl group parallel to tertiary amine group and both hydroxyl groups forming interaction with Cl⁻ ion (Fig. 1B **complex 1:1b**). The complex **1:1a** was stabilized by H-bond interaction between the carboxyl group of the acid and Cl⁻ ion ($d(\text{O}-\text{H}-\text{Cl}) = 1.928 \text{ \AA}$) and between OH group of the choline and carbonyl atom of the carboxyl group ($(\text{O}-\text{H}-\text{O}=\text{C}) = 1.814 \text{ \AA}$). The Cl⁻ was bound to choline, beside electrostatic Coulomb interaction, by two C–H–Cl H-bonds with characteristic $d(\text{C}-\text{H}-\text{Cl})$ distance of 2.42 \AA [27]. The acid formed also a weak intramolecular H-bond between its 3-OH group and the carboxyl group.

The **complex 1:1b** differed in the binding mode as there Cl⁻ ion was H-bonded by two OH groups, i.e. one from choline and 3-OH group of the acid ($d(\text{O}-\text{H}-\text{Cl})$ of 2.287 and 2.067 \AA , respectively). This time a strong intramolecular H-bond was formed between OH group in the carboxylic group and O atom of the 3-OH group with $d(\text{COOH}-\text{OH}-\text{C}) = 1.654 \text{ \AA}$. The other H-bond interactions were not so evident and

could not be easily detected due to an increase in the bond length or redshift of their vibration modes.

Similarly to 1:1 stoichiometry, we identified two possible arrangements of 2:1 complexes. The **complex 2:1a** was stabilized by two carboxyl groups forming H-bond with Cl⁻ ($d(\text{COOH}-\text{Cl})$ in the range of 1.98 to 2.04 \AA). One of the acids formed H-bond with OH group of the choline as in **complex 1:1a**. In the **complex 2:1b** (Fig. 1D) the Cl⁻ ion was being enclosed by two acids and choline with three H-bonds between respective OH groups (with $d(\text{OH}-\text{Cl})$ in the range of 2.07 to 2.15 \AA). In both acids the intramolecular H-bonds between COOH and 3-OH groups were observed as in the **complex 1:1b**.

Finally, we observed one type of the **3:1 and 4:1 complexes** (Fig. 1E, F). These complexes resembled **complex 2:1b**, with acid positioned in parallel to others and OH groups of acids and choline acting as H-bond donors in the O–H–Cl interactions. In **complex 3:1** the distances of OH–Cl bonds were in the range of 2.144–2.263 \AA and in case of the **complex 4:1** the $d(\text{OH}-\text{Cl})$ were in the range of 2.107–2.378 \AA . The OH group of the carboxyl groups formed predominantly internal H-bond interactions with the oxygen atom of the 3-OH group acting as an H-bond acceptor (average $d(\text{OH}-3-\text{O})$ distance of 1.669 \AA). In both **3:1 and 4:1 complexes** we observed intermolecular H-bond interaction between two carboxyl groups of two different acids (OH groups acting as H-bond donor and acceptor) with $d(\text{OH}-\text{O})$ distance range 1.785–1.803 \AA .

The analysis of the thermodynamics of complex formation revealed that all presented complexes were thermodynamically stable (ΔG of formation in the range of –51.5 to –135.5 kJ/mol of the complex). The binding mode represented by **complex 1:1b** and **complex 2:1b** (Fig. 1B and D) turned out to be more favourable than those observed for complexes **1:1a** and **2:1a** as the ΔG of binding for respective complexes were –52.4 and –98.6 kJ/mol vs. –51.5 and –86.2 kJ/mol. Although the overall ΔG value decreased with an increase of the complex size, the ΔG per molecule of acid gradually decreased from –52.4 kJ/mol (**1:1b**) to –33.9 kJ/mol (**4:1**, see Table 1S of the ESI for all data). Even though the gas-phase calculations cannot be directly used to describe DES behaviour in the condensed phase, we can expect the formation of similar complexes in the solution. As the calculated ΔG values did not differ very significantly, it is reasonable to assume that the distribution of various forms will be present in each of the investigated liquids with increasing occurrence of the higher complexes for the liquids with higher acid to choline chloride ratio.

3.3. Spectroscopic insights into hydrogen bond formation – theory vs experiment

Based on the calculated structures of complexes we were able to describe changes in IR and NMR spectra observed upon the formation of the DES. As indicated by our calculation the 3-OH groups of acids as well as OH group of choline is frequently involved in H-bond interaction with Cl⁻ ion. This results with deshielding of these protons and downfield shift of their NMR signals. The calculated H NMR signals of protons at 3-OH group that did not interact with Cl⁻ or carboxylic groups were in the range of 1.86–2.87 ppm, while signals of groups involved in H-bonds were in the range of 4.87 up to even 8.06 ppm (see Table S3). Signals of choline OH groups were between 2.95 and 5.78 ppm depending on the degree of interactions. A similar pattern was observed for DESs solutions in CDCl₃ when analysed by NMR (Fig. S3). We observed broad peaks in the range of 5.5–6.2 ppm arising from protons of OH groups belonging to (*R*)-3-hydroxyacids, which were found to interact with Cl⁻ ions in theoretical calculations. Likewise, the proton signals of choline hydroxylic groups were found in the range of 4.7–5.3 ppm. In both cases, the position of the signal varied and most probably depended on the strength of H-bonds and the dissolution of the compound in deuterated chloroform. However we did not observe any correlation between the magnitude of the signal shift and the DES type.

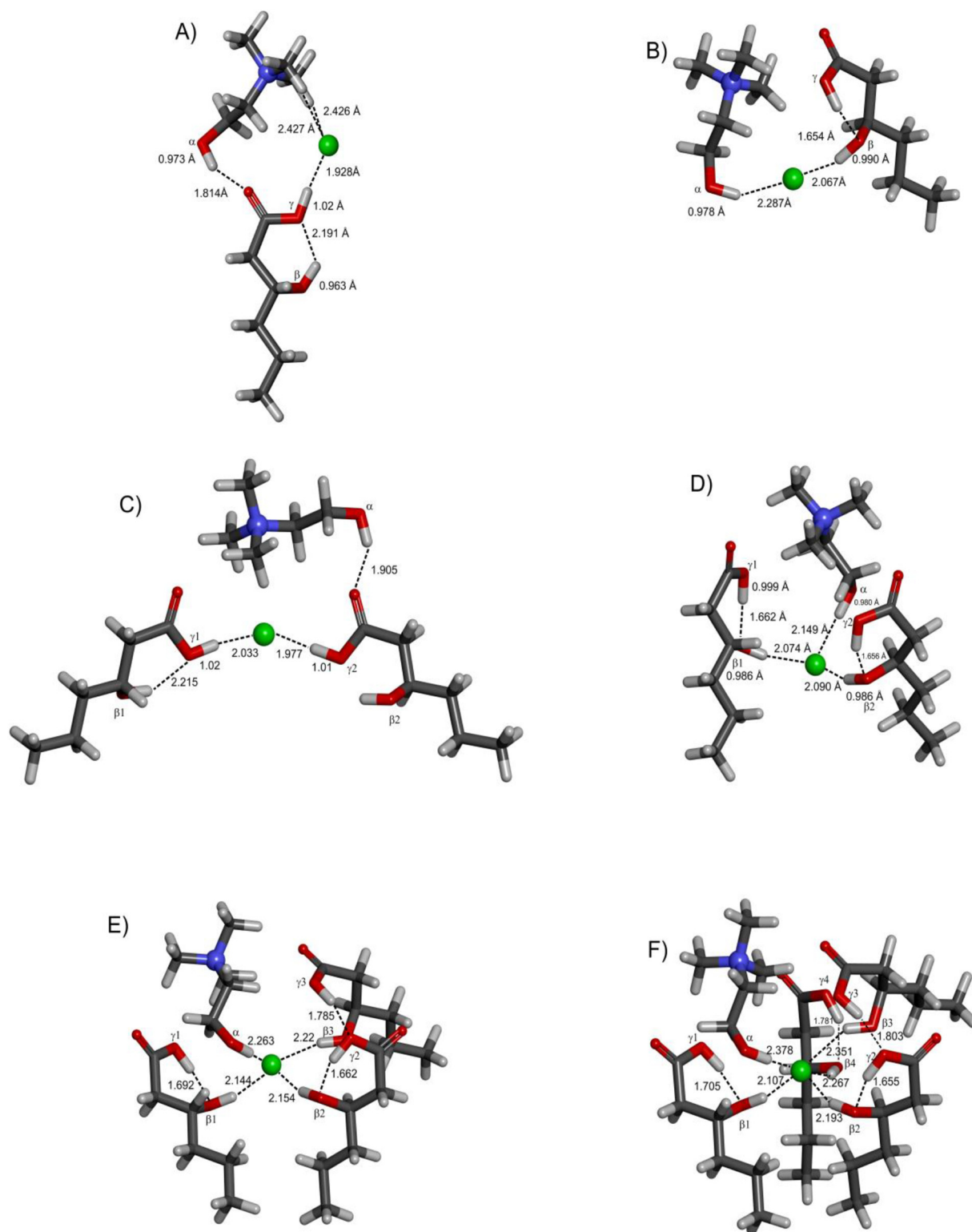


Fig. 1. Gas-phase optimized geometries of (*R*)-3-hydroxyhexanoic and choline chloride NADES: A) 1:1a, B) 1:1b C) 2:1a D) 2:1b, E) 3:1, F) 4:1; dashed line H-bond interactions; distances are provided in Å.

In IR we selected changes in ν stretching vibration of COO-H and O—H bonds to study the formation of H-bonds. The stretching frequencies of OH groups that do not form H-bond interaction were predicted to appear in the range of 3680–3716 cm^{-1} . In most cases, when these groups formed H-bond interactions with Cl^- or COOH, their frequencies were redshifted to 3200–3400 cm^{-1} region. These redshifts were stronger in the case of 3-OH groups of acids compared to OH group of choline.

Although in pure acids the COOH groups also form internal and external H-bond interrelations (which result in the redshift of vibration frequency) in DESs we observed significant shifts of the $\nu\text{COO-H}$ stretching modes to the range of 3000–3250 cm^{-1} and in some cases (e.g. **1:1a**, **2:1a**) even shifts to the range of 2870–2700 cm^{-1} . The vast majority of the theoretical predictions were mirrored in the experimental IR data (Fig. S4). There we observed a broad peak spanning from 3090 to

Table 1

Polynomial best-fit parameters for the dynamic viscosity-temperature relationship (A_d , B_d and C_d), including percentage deviation (α_d) and coefficient of determination (R^2) values and the kinematic viscosity-temperature relationship (A_k , B_k and C_k), including percentage deviation (α_k) and coefficient of determination (R^2) values.

	R3HA:ChCl	A_d	B_d	C_d	α_d (%)	R^2
Dynamic	1:1	1.0019	-670.87	112,440	0.451	1
	1.5:1	0.3365	-228.21	38,795	3.419	0.9983
	2:1	0.2271	-154.37	26,316	0.841	0.9995
	2.5:1	0.1912	-130.04	22,177	2.548	0.9995
	3:1	0.1981	-133.47	22,547	1.770	0.9987
	R3HA:ChCl	A_k	B_k	C_k	α_k (%)	R^2
Kinematic	1:1	0.9696	-649.22	108,813	1.392	0.9999
	1.5:1	0.3050	-206.98	35,214	3.750	0.9983
	2:1	0.2202	-149.71	25,531	1.902	0.9995
	2.5:1	0.1858	-126.41	21,566	3.299	0.9995
	3:1	0.1948	-131.25	22,171	1.945	0.9986

3680 cm^{-1} , which was assigned to H-bond forming OH-groups. The broadband associated with these peaks exhibit redshift when compared to the spectra of the 3-hydroxyacids [14].

Further, we identified characteristic band at 1716 cm^{-1} representing ν C=O, along with skeletal stretching vibrational signals

of choline moiety for the CH_2 bending (1477 cm^{-1}), CH_3 bending (1375 cm^{-1}) and at 1082 or 951 cm^{-1} , which based on the calculations can be attributed to ν Ξ and ν of the moiety N- CH_3 , respectively [28,29]. These were in good correlation with our previous study when we synthesized DES based on shorter hydroxyacids and choline chloride [14]. Moreover, the height ratio of bands at 1716 cm^{-1} to 951 cm^{-1} for each analyzed DES enabled quantitation of acid and choline component (Fig. S5). The analysis of this ratio yields a linear relationship ($R^2 = 0.94$) with respect to theoretical acid:choline ratio, confirming the stoichiometry of the (R)-3-hydroxyacids to choline in the synthesized mixtures.

3.4. Viscosity of DESs

Dynamic and kinematic viscosity measurements were conducted for the five synthesised DESs (Fig. 2). The expected trends of increasing viscosity with decreasing temperature and decreasing R3HA fraction in DES were in agreement with literature data [14,30,31]. It can be seen (Fig. 2 panel A and C) that the viscosity decreased with increasing temperature and was dependent on R3HA:ChCl ratio; with the lowest ratio (1:1) exhibiting the most rapid decrease (steepest relationship). There was perhaps a change in the gradient (at a constant temperature, panels

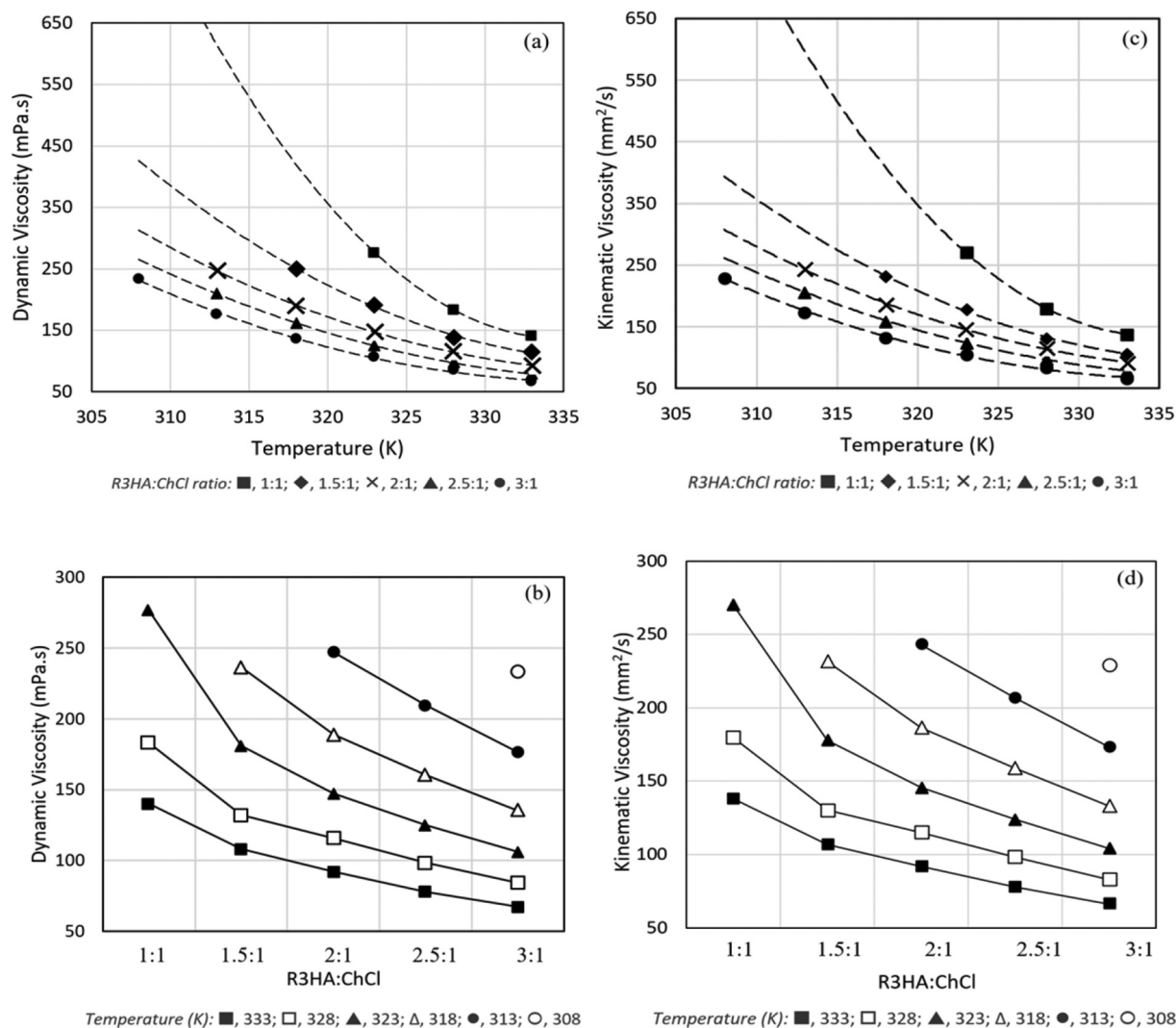


Fig. 2. Dynamic and kinematic viscosity of synthesised DESs. Panels: (a) Plot of dynamic viscosity vs. temperature for DESs with varying R3HA:ChCl ratio, including dashed polynomial fit trendlines; (b) Plot of dynamic viscosity vs. R3HA:ChCl ratio with varying temperature; (c) Plot of kinematic viscosity vs. temperature for DESs with varying R3HA:ChCl ratio, including dashed polynomial fit trendlines; (d) Plot of kinematic viscosity vs. R3HA:ChCl ratio with varying temperature. N.B. Error bars have been included but are not visible at the given scale.

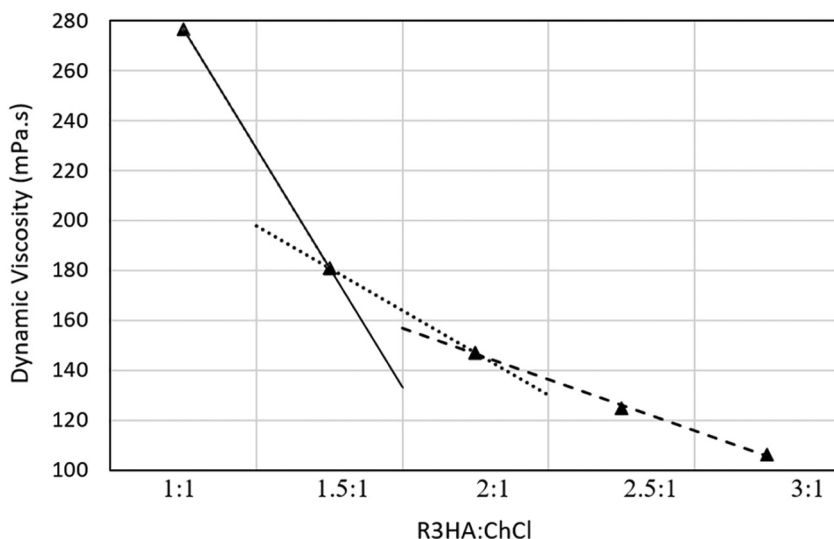


Fig. 3. Plot of dynamic viscosity vs. R3HA:ChCl ratio at 323 K, outlining the changes in linear trendline gradient.

B and D in Fig. 2, highlighted in Fig. 3) when the ratio increased from 1:1 to 2:1 and from 2:1 to 3:1.

The viscosity-temperature dependences were fitted using a polynomial relationship, with the best-fit parameters for dynamic (η_d) and kinematic (η_k) viscosity, according to Eq. (1), listed in Table 1.

$$\eta = AT^2 + BT + C \quad (1)$$

where η is the viscosity, A, B, C are the fitting parameters, T is the temperature in K.

Whilst the polynomial fits provide a relatively valid representation of the empirical data, with deviation of 0.451–3.750% and R^2 values of 0.9983–0.9999, the Vogel-Tamman-Fulcher (VTF) Arrhenius model, used extensively in the literature to fit viscosity-temperature data, can report deviation values less than one-tenth of a percent [31,32]. DES viscosity (η) as a function of temperature (T) was fitted accordingly to the VTF equation:

$$\eta = \lambda T^{0.5} \exp\left(\frac{-k}{T-T_0}\right) \quad (2)$$

Fitting the model to experimental data provided values of empirical constants k , the DES's kinetic pseudoactivation energy (kcal/mol) and T_0 , the ideal glass transition temperature (divergence temperature (K) for which system configurational energy disappears). The lowest observed viscosity in the dataset (high temperature limiting value) is denoted as λ . The optimized coefficients and relative deviations for the dynamic viscosity results are displayed in Table 2. The polynomial fit more accurately described the experimental data than the VTF model. This was reflected in the comparison of the relative deviations. The data provides a strong indication that the R3HA:ChCl DES follows a non-Arrhenius temperature dependence. For comparison, a Phenol:ChCl DES, which has been proved to exhibit Arrhenius behaviour, has

Table 2

Optimized VTF relative deviation (σ_{VTF}) and associated parameters, compared with relative deviation for dynamic viscosity polynomial fit (σ_d).

R3HA:ChCl	λ (mPa.s)	k (kcal/mol)	T_0 (K)	σ_{VTF} (%)	σ_d (%)
1:1	140.3	933.7	5.671	3.514	0.451
1.5:1	108.1	947.7	0.791	5.127	3.419
2:1	92.14	931.0	0.489	6.350	0.841
2.5:1	78.11	917.8	5.977	6.493	2.548
3:1	67.37	915.6	5.013	7.929	1.770

Density of DESs.

relative deviations no greater than 0.523% for all datasets [32], significantly smaller than the highest observed deviation of 7.929% in this VTF fitting.

The densities of DES formed between R3HA and ChCl are presented in Table 3 and Fig. 4. The density of DES was expected to decrease with an increase of temperature at a fixed molar ratio R3HA:ChCl. At a given temperature, the density of DES decreased with an increase of R3HA composition in the DES mixture. For example, for DES ratio 1:1 the values decreased linearly from 1.045 to 1.0154 g/cm³, and for ratio 3:1 only from 1.0278 to 1.0045 g/cm³. The density decreased as the fraction of the heavier component (ChCl). The trend in density vs. R3HA:ChCl ratio was consistent across the entire testing range and proportional to the decrease in mass from a decrease of the ChCl fraction. A greater decrease in density was observed at the transition from 1:1 to 2:1 structure than to 3:1. This may indicate a change in the volume structure of the mixture being formed. The density-temperature dependence has been fitted using a polynomial fit (Eq. (3)) and superimposed on the obtained data (Fig. 4).

$$\rho = A_p T^2 + B_p T + C_p \quad (3)$$

where ρ is the density in g/cm³, A_p , B_p , C_p are the fitting parameters, T is the temperature in K. The empirical parameters, deviation, and coefficient of determination were displayed in Table 4. For all measurements the relative deviations (σ) were very small, between 0.0027 and 0.1610. The R^2 was found to be larger than 0.9998, which indicated that the density-temperature relationship was linear.

Measurements of liquid contact angles on solid mica, glassy carbon and Teflon surfaces allowed us to study the wetting properties of DESs. We chose materials with different polarity and hydrophobicity to obtain a better characteristic of wetting and surface properties of

Table 3

Matrix of temperature and R3HA:ChCl ratio dependence on density.

R3HA:ChCl	Temperature (K)							
	298	303	308	313	318	323	328	333
	Density (g/cm ³)							
1:1	1.046	1.042	1.038	1.034	1.029	1.025	1.020	1.015
1.5:1	1.037	1.033	1.029	1.025	1.021	1.018	1.013	1.010
2:1	1.028	1.025	1.022	1.018	1.015	1.012	1.008	1.005
2.5:1	1.024	1.021	1.018	1.015	1.011	1.008	1.005	1.001
3:1	1.022	1.019	1.016	1.013	1.009	1.006	1.003	1.000

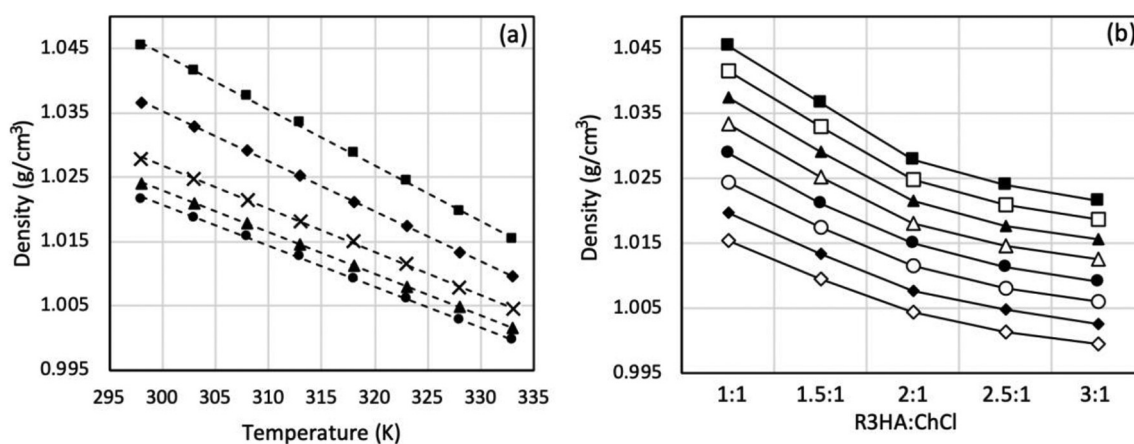


Fig. 4. (a) Plot of density vs. temperature for DESs with R3HA:ChCl ratios: ■, 1:1; ◆, 1.5:1; ×, 2:1; ▲, 2.5:1; ●, 3:1, including dashed polynomial fit trend lines (see Table 3). (b) Plot of density vs. R3HA:ChCl ratio with temperatures (K): ■, 333; □, 328; ▲, 323; △, 318; ●, 313; ○, 308; ◆, 303; ◇, 298.

synthesised NADES. Before the experiments we examined the properties of used solid materials by the surface electron microscopy SEM observations and surface free energy evaluations. Photographs of these surfaces are presented in ESI (Figs. S6–S8). The most uniform surface was observed for mica, whereas the polished glassy carbon and Teflon plates presented more disturbed interfaces. The surface free energy of the studied solid materials was analysed using the Owens-Wendt method [33,34]. For this purpose, two liquids – polar water and non-polar diiodomethane (DIM) – were used to determine the surface free energy of examined material (water $\delta = 72.30 \text{ mN m}^{-1}$, diiodomethane $\delta = 50.80 \text{ mN m}^{-1}$; Figs. S1–S3, Table S1). The qualitative analysis of data allowed us to conclude that the DESs showed physicochemical similarity both for polar (mica) as well as for hydrophobic dispersive surfaces (glassy carbon and in some cases Teflon) (Fig. 5). Similar observations were already reported in the case of some ionic liquids (ILs), i.e. [C8MIM][NTf2], which presented a contact angle of $49.58^\circ \pm 0.21^\circ$ on Teflon, while it was $22.84^\circ \pm 0.23^\circ$ on silica plate [35]. The authors proved that the longer alkyl chain imidazolium cation units of [C8MIM][NTf2] presented a lower contact angle with Teflon than their shorter counterparts of [C4MIM][NTf2] (66.25°). It indicated the effect of dispersive interactions in the definition of contact angle on Teflon or other hydrophobic material. However, the hypothesis of dispersive interactions between short carbon chain ILs and polar surfaces presented in [35] is impossible to defend in the case of our R3HA-based DESs (6 to 14 carbon in the chain). In our case, we must consider that the low contact angles on the polar surface (mica) are the result of hydrogen-bond interaction between DESs and polar surface [36].

In our studies we examined five various DESs with a different molar ratio between hydrophobic R3HA part and hydrophilic choline 1:1; 1.5:1; 2:1; 2.5:1 and 3:1. As seen from Fig. 5, the variation of the ratios of the hydrophobic to hydrophilic components had a minor effect on the surface properties of DESs (contact angles of DESs on various surfaces). The polar component of the DESs interactions (determined by

contact angle on mica) was almost constant (within experimental error accuracy). In the case of the experiment with Teflon the wetting angles were in the range between $50.3^\circ \pm 1.7^\circ$ for DES 1:1 and $48.2^\circ \pm 1.5^\circ$ for 3:1 M ratio, respectively. When obtained results were compared to the wettability of Teflon with DESs of a narrower R3HA distribution ((*R*)-3-hydroxyheptanoic and (*R*)-3-hydroxynonanoic), which was $55.9^\circ \pm 3.3^\circ$ [14], one can conclude that increasing the ratio of more hydrophobic R3HA to hydrophilic ChCl leads to the increase of wetting ability of the non-polar surface. The results for glassy carbon (contact angle in range 17.5° – 22.0°), which has less hydrophobic properties than Teflon, are in good agreement with data obtained for Teflon and mica. Here, both polar (hydrogen bond) and dispersive interactions between DES and glassy carbon plate must be considered. Concluding, the synthesized DESs reveal their slightly polar and hydrophobic character when tested on these three surfaces.

3.5. Solubility of DESs

Numerical solubility results, including absolute uncertainties, were presented in Table 5, whereas the experimental results depicting mixtures after mixing the liquids together followed by centrifugation were shown in Fig. 6. Both 1:1 and 2:1 R3HA:ChCl DESs had negligible solubility in water. Similarly, the evidence suggested that the DESs were only partially soluble in hexane. On the other hand, the tested mixtures were highly soluble in methanol and chloroform. As a result of their intramolecular, highly polar, hydrogen bonding networks, DES species would be expected to interact with each other and solvent species via polar attractions. The solubility in the solvent species investigated can, therefore, be explained in terms of the polarity index (PI), a scale describing the relative polarity of a species between 0 (non-polar) to 10 (very polar). The DESs solubility in methanol (polarity index 5.1) suggests that polar forces are indeed influencing its solubility. The increase in solubility from methanol to chloroform however suggests that R3HA:ChCl's polarity, and hence compatibility with like-for-like solvents, lies further toward the non-polar end of the spectrum. The observation is reinforced by the DESs partial solubility in non-polar *n*-hexane. Although highly polar H-bonding exists within the DESs structure, the larger proportion of low polarity bonding (e.g. C–C, C–H and C=O) somewhat outweighs the polar effects. It can, therefore, be concluded that R3HA:ChCl's polarity index lies in the range of 0–4.1, closer to the mildly polar end. The influence of the balance between polar and non-polar bonding on solubility is also evident when comparing the 1:1 and 2:1 DESs. For the partially polar solvents, methanol and chloroform, there is an appreciable difference between the solubility. The solubility of the 1:1 DES, which has a higher

Table 4

Polynomial best-fit parameters for the density-temperature relationship (A_p , B_p , & C_p) including percentage deviation (σ) and coefficient of determination (R^2) values.

R3HA:ChCl	A_p (10^{-6})	B_p (10^{-3})	C_p	σ (%)	R^2
1:1	−2.340	0.612	1.0711	0.0147	0.9999
1.5:1	−0.783	−0.285	1.1913	0.0126	0.9999
2:1	−1.410	0.218	1.0878	0.0344	0.9998
2.5:1	−0.740	−0.178	1.1428	0.0027	1
3:1	−1.160	0.100	1.0953	0.1610	0.9998

Wetting properties of DESs.


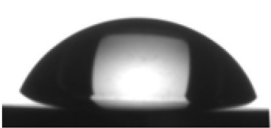
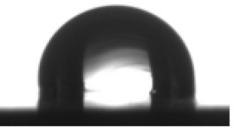



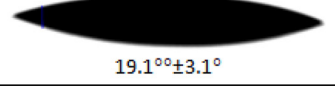
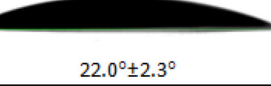
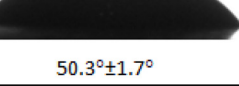
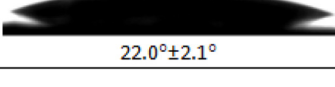
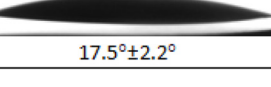

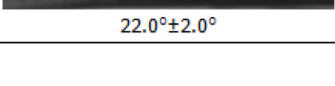
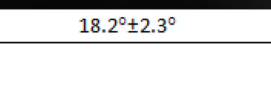
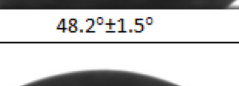
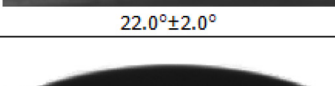
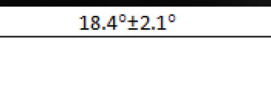

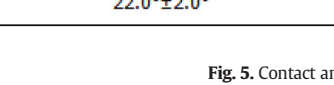
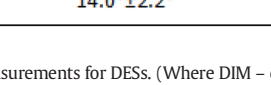
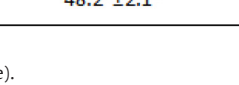
	Mica	Glassy carbon	Teflon
H ₂ O	 0.0°	 67.1°±0.6°	 94.2°±0.5°
DIM	 47.0°±2.3°	 34.3°±2.4°	 74.2°±0.6°
1:1	 19.1°±3.1°	 22.0°±2.3°	 50.3°±1.7°
1.5:1	 22.0°±2.1°	 17.5°±2.2°	 49.6°±1.3°
2:1	 22.0°±2.0°	 18.2°±2.3°	 48.2°±1.5°
2.5:1	 22.0°±2.0°	 18.4°±2.1°	 48.4°±1.8°
3:1	 22.0°±2.0°	 14.0°±2.2°	 48.2°±2.1°

Fig. 5. Contact angle measurements for DESs. (Where DIM – diiodomethane).

proportion of polar to non-polar bonding, is greater than the more non-polar crowded 2:1 DES.

4. Conclusions

The combination of theoretical modelling and spectroscopic techniques allowed a more in-depth understanding of molecular interactions taking place upon DES complexes formations. We have shown that both carboxylic acid and choline act as H-bond donors via their OH groups with Cl⁻ ions acting as H-bond acceptors. Although

experimental NMR spectra deliver information of DES solutions in CDCl₃ and not for pure DESs, they demonstrated a significant downfield shift of signals attributed to protons from OH group. These shifts were sensitive to DES composition and were in qualitative agreement with our calculations. Similarly, the prediction of IR spectra facilitated the assignment of the diagnostic bands in the experimental spectra, which resulted in quantitative confirmation of DES stoichiometry. We could also attribute the redshift of broad O—H stretching band predominantly to the newly formed H-bonds between 3-OH groups and Cl⁻.

A variety of analytical techniques were utilised in the physicochemical profiling of the DESs. Results of viscosity measurement proved that as both the temperature and fraction of hydrogen bond donor (R3HA) in the DES increased, the viscosity of the sample gradually and smoothly decreased. Density was also found to increase monotonically with decreasing temperature. Whilst similarly to the viscosity vs. ratio dependence the density increased with decreasing R3HA fraction, however there was no noticeable deviation from the observed trend when changing from 2:1 to 1:1; suggesting that the change of bonding mechanisms has no appreciable influence on the DESs occupied volume. It was shown that the R3HA:ChCl DESs were insoluble in highly polar water but soluble in mildly polar solvents methanol and chloroform. There was also a limited degree of solubility in non-polar *n*-hexane, suggesting that the trade-off of polar and non-polar bonding within the DESs structure influences its solubility. This character was also evident from the preformed wettability measurements, suggesting that these solvents are of polar and slight hydrophobic character.

Table 5
Solubility and polarity of 1:1 and 2:1 R3HA:Choline Chloride DESs (at STP) in terms of g/ml solution and g/ml solvent, including absolute and percentage uncertainty.

Solvent	Solvent polarity index	DES ratio HBD:HBA	Solubility (DES g/ml solvent)	Standard error (DES g/ml solvent)
Water	9.0	1:1	0.0006	±0.0002
		2:1	0.0005	±0.0002
Methanol	5.1	1:1	0.1827	±0.0028
		2:1	0.1548	±0.0025
Chloroform	4.1	1:1	0.3275	±0.0068
		2:1	0.2779	±0.0157
<i>n</i> -Hexane	0.0	1:1	0.0350	±0.0025
		2:1	0.0260	±0.0010

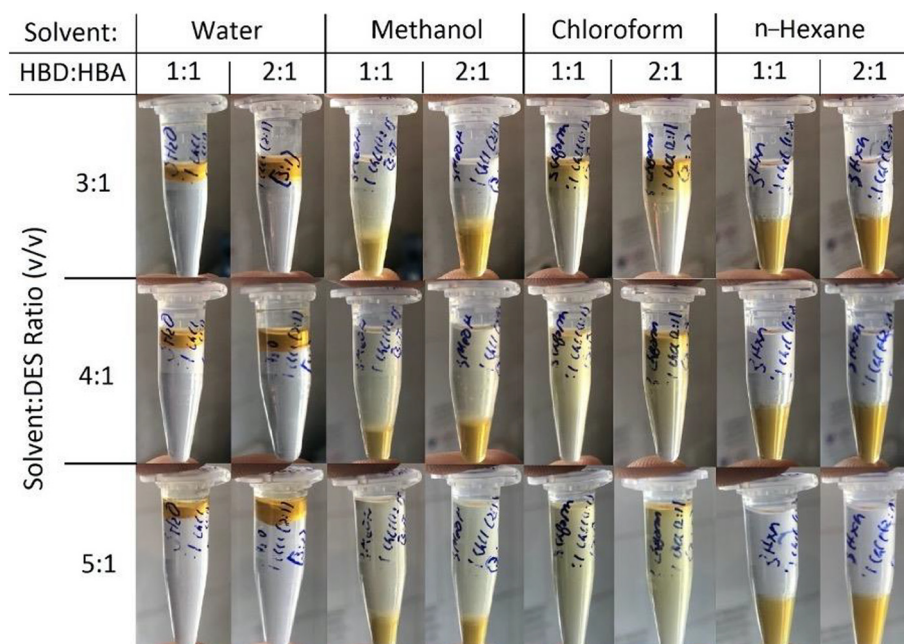


Fig. 6. Matrix showing dissolution of 1:1 and 2:1 R3HA:ChCl DES over increasing solvent ratios. Yellow phase is observed for tested DESs in case of water and hexane, where the transparent phase reveals no mixing with these solvents. It can be clearly seen that the liquids mixed in great extent when chloroform was used, whereas a partial solubilisation can be seen when methanol was used.

This work provides an in-depth characterization of biomass-derived natural deep eutectic solvents. The described viscosity and density behaviours, accompanied by wettability and solubility properties, will allow in the future for finding areas of applications where these selective systems can replace traditional petroleum-based, and in most cases harmful solvents.

CRedit authorship contribution statement

Lyall Archer: Methodology, Validation, Formal analysis, Investigation, Visualization, Writing - original draft. **Barbara Jachimska:** Methodology, Supervision, Writing - review & editing. **Marcel Krzan:** Investigation, Visualization, Writing - original draft, Writing - review & editing. **Maciej Szaleniec:** Investigation, Formal analysis, Writing - original draft, Writing - review & editing. **Edyta Hebda:** Investigation, Validation. **Paulina Radzik:** Investigation, Data curation. **Krzysztof Pielichowski:** Supervision, Writing - review & editing. **Maciej Guzik:** Conceptualization, Methodology, Investigation, Writing - original draft, Writing - review & editing, Resources, Supervision, Project administration, Funding acquisition.

Declaration of competing interest

Authors declare no conflict of interests.

Acknowledgments

This research was funded by the statutory research fund of Jerzy Haber Institute of Catalysis and Surface Chemistry Polish Academy of Sciences. Calculations were supported by PL-Grid Infrastructure (AGH CYFRONET).

Appendix A. Supplementary data

Supplementary data to this article can be found online at <https://doi.org/10.1016/j.molliq.2020.113680>.

References

- Y. Dai, R. Verpoorte, Y.H. Choi, Natural deep eutectic solvents providing enhanced stability of natural colorants from safflower (*Carthamus tinctorius*), Food Chem. 159 (2014) 116–121, <https://doi.org/10.1016/j.foodchem.2014.02.155>.
- A.K. Kumar, S. Sharma, E. Shah, A. Patel, Technical assessment of natural deep eutectic solvent (NADES) mediated biorefinery process: a case study, J. Mol. Liq. 260 (2018) 313–322, <https://doi.org/10.1016/j.molliq.2018.03.107>.
- Y. Xie, H. Liu, L. Lin, M. Zhao, L. Zhang, Y. Zhang, Y. Wu, Application of natural deep eutectic solvents to extract ferulic acid from *Ligusticum chuanxiong* Hort with microwave assistance, RSC Adv. 9 (2019) 22677–22684, <https://doi.org/10.1039/c9ra02665g>.
- G. Sed, A. Ciccì, P.G. Jessop, M. Bravi, A novel switchable-hydrophilicity, natural deep eutectic solvent (NaDES)-based system for bio-safe biorefinery, RSC Adv. 8 (2018) 37092–37097, <https://doi.org/10.1039/c8ra08536f>.
- K. Haražna, K. Walas, P. Urbańska, T. Witko, W. Snoch, A. Siemek, B. Jachimska, M. Krzan, B.D. Napruszewska, M. Witko, S. Bednarz, M. Guzik, Polyhydroxyalkanoate-derived hydrogen-bond donors for the synthesis of new deep eutectic solvents, Green Chem. 21 (2019) 3116–3126, <https://doi.org/10.1039/c9gc00387h>.
- S. Nejrotti, M. Iannicelli, S.S. Jamil, D. Arnodo, M. Blangetti, C. Prandi, Natural deep eutectic solvents as an efficient and reusable active system for the Nazarov cyclization, Green Chem. 22 (2020) 110–117, <https://doi.org/10.1039/c9gc03465j>.
- Y. Zou, X. Xin, H. Xu, H. Yuan, X. Li, Y. Yu, G. Zhao, Highly efficient bioconversion of flavonoid glycosides from citrus-processing wastes in solvent-buffer systems, Green Chem. 22 (2020) 3196–3207, <https://doi.org/10.1039/d0gc00669f>.
- Á. Mourelle-Insua, I. Lavandera, V. Gotor-Fernández, A designer natural deep eutectic solvent to recycle the cofactor in alcohol dehydrogenase-catalysed processes, Green Chem. 21 (2019) 2946–2951, <https://doi.org/10.1039/c9gc00318e>.
- M. Feng, X. Lu, J. Zhang, Y. Li, C. Shi, L. Lu, S. Zhang, Direct conversion of shrimp shells to O-acylated chitin with antibacterial and anti-tumor effects by natural deep eutectic solvents, Green Chem. 21 (2019) 87–98, <https://doi.org/10.1039/c8gc02506a>.
- C. Mukesh, R. Gupta, D.N. Srivastava, S.K. Nataraj, K. Prasad, Preparation of a natural deep eutectic solvent mediated self polymerized highly flexible transparent gel having super capacitive behaviour, RSC Adv. 6 (2016) 28586–28592, <https://doi.org/10.1039/c6ra03309a>.
- M.A. Kadhom, G.H. Abdullah, N. Al-Bayati, Studying two series of ternary deep eutectic solvents (choline chloride-urea-glycerol) and (choline chloride-malic acid-glycerol), synthesis and characterizations, Arab. J. Sci. Eng. 42 (2017) 1579–1589, <https://doi.org/10.1007/s13369-017-2431-4>.
- Z. Maugeri, P. Domínguez De María, Novel choline-chloride-based deep-eutectic-solvents with renewable hydrogen bond donors: Levulinic acid and sugar-based polyols, RSC Adv. 2 (2012) 421–425, <https://doi.org/10.1039/c1ra00630d>.
- K. Radošević, M. Cvjetko Bubalo, V. Gaurina Srček, D. Grgas, T. Landeka Dragičević, I. Radojčić Redovniković, Evaluation of toxicity and biodegradability of choline chloride based deep eutectic solvents, Ecotoxicol. Environ. Saf. 112 (2015) 46–53, <https://doi.org/10.1016/j.ecoenv.2014.09.034>.
- K. Haražna, K. Walas, P. Urbańska, T. Witko, W. Snoch, A. Siemek, B. Jachimska, M. Krzan, B.D. Napruszewska, M. Witko, S. Bednarz, M. Guzik, Polyhydroxyalkanoate-

- derived hydrogen-bond donors for the synthesis of new deep eutectic solvents, *Green Chem.* 21 (2019) 3116–3126, <https://doi.org/10.1039/C9GC00387H>.
- [15] A. Steinbüchel, H.E. Valentin, Diversity of bacterial polyhydroxyalkanoic acids, *FEMS Microbiol. Lett.* 128 (1995) 219–228.
- [16] J. Nikodinovic-Runic, M. Guzik, S.T. Kenny, R. Babu, A. Werker, K.E.O. Connor, Carbon-rich wastes as feedstocks for biodegradable polymer (Polyhydroxyalkanoate) production using bacteria, *Adv. Appl. Microbiol.* (2013) 139–200, <https://doi.org/10.1016/B978-0-12-407673-0.00004-7>.
- [17] C. Ruiz, S.T. Kenny, R. Babu P, M. Walsh, T. Narancic, K.E. O'Connor, High cell density conversion of hydrolysed waste cooking oil fatty acids into medium chain length polyhydroxyalkanoate using *Pseudomonas putida* KT2440, *Catalysts* 9 (2019) 468, <https://doi.org/10.3390/catal9050468>.
- [18] M. Walsh, K. O'Connor, R. Babu, T. Woods, S. Kenny, Plant oils and products of their hydrolysis as substrates for polyhydroxyalkanoate synthesis, *Chem. Biochem. Eng. Q.* 29 (2015) 123–133, <https://doi.org/10.15255/CABEQ.2014.2252>.
- [19] P.K. Sharma, R.I. Munir, T. de Kievit, D.B. Levin, Synthesis of polyhydroxyalkanoates (PHAs) from vegetable oils and free fatty acids by wild-type and mutant strains of *Pseudomonas chlororaphis*, *Can. J. Microbiol.* 63 (2017) 1009–1024, <https://doi.org/10.1139/cjm-2017-0412>.
- [20] K. Sofińska, J. Barbasz, T. Witko, J. Dryzek, K. Harażna, M. Witko, J. Kryściak-Czerwenka, M. Guzik, Structural, topographical, and mechanical characteristics of purified polyhydroxyoctanoate polymer, *J. Appl. Polym. Sci.* 136 (2019), 47192, <https://doi.org/10.1002/app.47192>.
- [21] J. Radivojevic, S. Skaro, L. Senerovic, B. Vasiljevic, M. Guzik, S.T. Kenny, V. Maslak, J. Nikodinovic-Runic, K.E. O'Connor, Polyhydroxyalkanoate-based 3-hydroxyoctanoic acid and its derivatives as a platform of bioactive compounds, *Appl. Microbiol. Biotechnol.* 100 (2016) 161–172, <https://doi.org/10.1007/s00253-015-6984-4>.
- [22] A.D. Becke, Density-functional thermochemistry. III. The role of exact exchange, *J. Chem. Phys.* 98 (1993) 5648–5652, <https://doi.org/10.1063/1.464913>.
- [23] G.A. Petersson, A. Bennett, T.G. Tensfeldt, M.A. Al-Laham, W.A. Shirley, J. Mantzaris, A complete basis set model chemistry. I. The total energies of closed-shell atoms and hydrides of the first-row elements, *J. Chem. Phys.* 89 (1988) 2193–2218, <https://doi.org/10.1063/1.455064>.
- [24] S. Grimme, J. Antony, S. Ehrlich, H. Krieg, A consistent and accurate ab initio parametrization of density functional dispersion correction (DFT-D) for the 94 elements H–Pu, *J. Chem. Phys.* 132 (2010), 154104, <https://doi.org/10.1063/1.3382344>.
- [25] K. Wolinski, J.F. Hinton, P. Pulay, Efficient implementation of the gauge-independent atomic orbital method for NMR chemical shift calculations, *J. Am. Chem. Soc.* 112 (1990) 8251–8260, <https://doi.org/10.1021/ja00179a005>.
- [26] P. Talik, U. Hubicka, The DSC approach to study non-freezing water contents of hydrated hydroxypropylcellulose (HPC): a study over effects of viscosity and drug addition, *J. Therm. Anal. Calorim.* 132 (2018) 445–451, <https://doi.org/10.1007/s10973-017-6889-9>.
- [27] T. Steiner, Hydrogen-bond distances to halide ions in organic and organometallic crystal structures: up-to-date DATABASE study, *Acta Crystallogr. Sect. B Struct. Sci.* 54 (1998) 456–463, <https://doi.org/10.1107/S0108768197014821>.
- [28] N. Delgado-Mellado, M. Larriba, P. Navarro, V. Rigual, M. Ayuso, J. García, F. Rodríguez, Thermal stability of choline chloride deep eutectic solvents by TGA/FTIR-ATR analysis, *J. Mol. Liq.* 260 (2018) 37–43, <https://doi.org/10.1016/j.molliq.2018.03.076>.
- [29] M.H. Shafie, R. Yusof, C.Y. Gan, Synthesis of citric acid monohydrate-choline chloride based deep eutectic solvents (DES) and characterization of their physicochemical properties, *J. Mol. Liq.* 288 (2019), 111081, <https://doi.org/10.1016/j.molliq.2019.111081>.
- [30] A.P. Abbott, R.C. Harris, K.S. Ryder, C. D'Agostino, L.F. Gladden, M.D. Mantle, Glycerol eutectics as sustainable solvent systems, *Green Chem.* 13 (2011) 82–90, <https://doi.org/10.1039/c0gc00395f>.
- [31] A. Yadav, S. Pandey, Densities and viscosities of (choline chloride + urea) deep eutectic solvent and its aqueous mixtures in the temperature range 293.15 K to 363.15 K, *J. Chem. Eng. Data* 59 (2014) 2221–2229, <https://doi.org/10.1021/je5001796>.
- [32] W. Guo, Y. Hou, S. Ren, S. Tian, W. Wu, Formation of deep eutectic solvents by phenols and choline chloride and their physical properties, *J. Chem. Eng. Data* 58 (2013) 866–872, <https://doi.org/10.1021/je300997v>.
- [33] A. Rudawska, E. Jacniacka, Analysis for determining surface free energy uncertainty by the Owen-Wendt method, *Int. J. Adhes. Adhes.* 29 (2009) 451–457, <https://doi.org/10.1016/j.ijadhadh.2008.09.008>.
- [34] D.K. Owens, R.C. Wendt, Estimation of the surface free energy of polymers, *J. Appl. Polym. Sci.* 13 (1969) 1741–1747, <https://doi.org/10.1002/app.1969.070130815>.
- [35] G.V.S.M. Carrera, C.A.M. Afonso, L.C. Branco, Interfacial properties, densities, and contact angles of task specific ionic liquids, *J. Chem. Eng. Data* (2010) 609–615, <https://doi.org/10.1021/je900502s>.
- [36] M.M. Pereira, K.A. Kurnia, F.L. Sousa, N.J.O. Silva, J.A. Lopes-Da-Silva, J.A.P. Coutinho, M.G. Freire, Contact angles and wettability of ionic liquids on polar and non-polar surfaces, *Phys. Chem. Phys.* 17 (2015) 31653–31661, <https://doi.org/10.1039/c5cp05873b>.